

# UNDERSAMPLED PHASE RETRIEVAL WITH IMAGE PRIORS

Stanislas Ducotterd, Zhiyuan Hu, Michael Unser, Jonathan Dong

Biomedical Imaging Group, École polytechnique fédérale de Lausanne, Lausanne, Switzerland

## ABSTRACT

Phase retrieval seeks to recover a complex signal from amplitude-only measurements, a challenging nonlinear inverse problem. Current theory and algorithms often ignore signal priors. By contrast, we evaluate here a variety of image priors in the context of severe undersampling with structured random Fourier measurements. Our results show that those priors significantly improve reconstruction, allowing accurate reconstruction even below the weak recovery threshold.

**Index Terms**— Inverse Problems, Phase Retrieval, Image Priors, Optimization, Regularization

## 1. INTRODUCTION

In many areas of science and engineering, one requires to recover an object of interest from indirect measurements. Within that context, phase retrieval is a particularly challenging nonlinear problem that aims at reconstruction of a complex signal  $\mathbf{x}$  from amplitude-only measurements [1].

This formulation arises in diverse applications, including x-ray crystallography, astronomical imaging [2], ptychography [3, 4], and Fourier ptychography [5, 6].

Random phase retrieval considers measurement matrices with independent random entries, which makes the study of exact recovery and algorithmic performance theoretically tractable [7, 8]. Recent works preserve these guarantees while reducing the computational cost. They achieve this by replacing dense randomness with structured transforms combined with random diagonal matrices [9]. Yet, this line of work largely ignores prior knowledge about natural signals, which can significantly improve recovery.

Image priors range from explicit sparsity-based regularizers such as total variation (TV) [10] to implicit ones embedded in powerful denoisers like DRUNet [11], integrated into iterative schemes via the plug-and-play (PnP) framework. Recent works seek to combine both the theoretical properties of the former with the empirical performance of the latter by learning explicit regularizers [12, 13, 14]. The random measurement model provides a well-characterized set-

ting to benchmark such strategies within the context of phase retrieval.

Beyond the scope of this study are generative frameworks, including adversarial, deep image prior, and diffusion models [15, 16, 17, 18]. We also refer to [19, 20] for the use of implicit and explicit regularizers in a more standard oversampled framework of phase retrieval.

In this work, we evaluate TV, the multivariate fields of experts (MFoE), and DRUNet, thus spanning a wide spectrum of priors. We show that the introduction of priors yields substantial gains and enables accurate recoveries under extreme undersampling. In particular, MFoE surpasses both TV and DRUNet, which suggests that principled explicit regularizers may be especially well-suited to nonlinear inverse problems like phase retrieval. The code is available on Github<sup>1</sup>.

## 2. PROBLEM DEFINITION

Our aim is to recover an  $n$ -dimensional complex signal  $\mathbf{x} \in \mathbb{C}^n$  from an  $m$ -dimensional real measurement vector  $\mathbf{y} \in \mathbb{R}^m$  obtained through the nonlinear forward model

$$\mathbf{y} = |\mathbf{S}\mathbf{F}\mathbf{D}\mathbf{x}| + \mathbf{n}, \quad (1)$$

where

- the entries of the known random diagonal matrix  $\mathbf{D} \in \{\pm 1\}^{n \times n}$  are drawn i.i.d. from  $\{-1, +1\}$  with equal probability;
- the discrete Fourier transform matrix is  $\mathbf{F} \in \mathbb{C}^{n \times n}$ ;
- the subsampling mask  $\mathbf{S} \in \{0, 1\}^{n \times n}$  is diagonal, where each diagonal entry is drawn i.i.d. from a Bernoulli distribution with parameter  $\alpha$ ;
- the Gaussian noise with noise level  $\sigma_{\mathbf{n}}$  is  $\mathbf{n} \sim \mathcal{N}(\mathbf{0}, \sigma_{\mathbf{n}}^2 \mathbf{I})$ .

The operator  $|\cdot|$  denotes the component-wise modulus. Formally,  $\mathbf{y}$  is in  $\mathbb{R}^n$  with  $m$  nonzero entries, but we identify it with  $\mathbb{R}^m$  by discarding the zero components. The operators  $\mathbf{D}$  and  $\mathbf{F}$  accurately model the combination of a diffuser and a lens in optical systems [1, 9].

A key hyperparameter is the sampling ratio  $\alpha$ . Smaller values of  $\alpha$  correspond to severe undersampling, making the

Stanislas Ducotterd acknowledges funding from the European Research Council (Grant Agreement - Project No 101020573 FunLearn). Zhiyuan Hu and Jonathan Dong acknowledge funding from the Swiss National Science Foundation (Grant PZ00P2\_216211).

<sup>1</sup><https://github.com/StanislasDucotterd/undersampled-phase-retrieval>

recovery problem increasingly harder. In this work, we investigate sampling ratios  $\alpha \in \{k/10\}_{k=1}^{10}$  with noiseless measurements, as well as noisy measurements with  $\sigma_{\mathbf{n}} \in \{0.001, 0.01, 0.1, 1\}$  without undersampling. Note that, below the weak recovery threshold  $\alpha_{\text{WR}} = 1$ , no information about  $\mathbf{x}$  is recoverable without prior information [7].

Structured random models generally correspond to cascades of Fourier and diagonal matrices of arbitrary depth. Prior works show that at least two layers (i.e.,  $\mathbf{FD}_2\mathbf{FD}_1$ ) are required to emulate dense models without prior knowledge [9]. Nonetheless, we find that even the simpler one-layer setup in (1) benefits significantly from regularization.

### 3. METHODS

#### 3.1. Data-Fitting Term and Its Proximal Operator

To address the phase retrieval problem, we adopt iterative schemes that alternately reduce the data-fidelity term

$$f(\mathbf{x}) = \frac{1}{2} \|\mathbf{SFD}\mathbf{x} - \mathbf{y}\|_2^2 \quad (2)$$

and enforce prior information on the solution.

The measurement operators we consider have the general form  $\mathbf{SU}$ , where  $\mathbf{S}$  is a binary sampling mask (Section 2) and  $\mathbf{U}$  is unitary. In this setting, iterative methods can be formulated using the proximal operator of  $f$ , defined as  $\text{prox}_{\lambda f}(\mathbf{x}) = \arg \min_{\mathbf{z} \in \mathbb{C}^n} \frac{1}{2} \|\mathbf{z} - \mathbf{x}\|_2^2 + \lambda f(\mathbf{z})$ .

**Theorem 1.** *The proximal operator of the data-fitting term  $f(\mathbf{x}) = \frac{1}{2} \|\mathbf{SU}\mathbf{x} - \mathbf{y}\|_2^2$  can be expressed as*

$$\text{prox}_{\lambda f}(\mathbf{x}) = \mathbf{U}^H \mathbf{S} \left( \frac{1}{1+\lambda} \mathbf{U}\mathbf{x} + \frac{\lambda}{1+\lambda} \mathbf{y} e^{j \arg(\mathbf{U}\mathbf{x})} \right) + \mathbf{U}^H (\mathbf{I} - \mathbf{S}) \mathbf{U}\mathbf{x}. \quad (3)$$

*Proof.* For the scalar problem,

$$\text{prox}_{\frac{\lambda}{2}(|\cdot| - y)^2}(x) = \arg \min_{z \in \mathbb{C}} \frac{1}{2} |z - x|^2 + \frac{\lambda}{2} (|z| - y)^2 \quad (4)$$

$$= \arg \min_{z \in \mathbb{C}} |z|^2 + |x|^2 + \lambda (|z| - y)^2 - 2|z||x| \cos(\arg z - \arg x) \quad (5)$$

and the only term depending on  $\arg z$  is minimized by setting  $\arg z = \arg x$ . Substituting the phase, one can compute the optimal magnitude, which yields

$$\text{prox}_{\frac{\lambda}{2}(|\cdot| - y)^2}(x) = \frac{1}{1+\lambda} x + \frac{\lambda}{1+\lambda} y e^{j \arg x}. \quad (6)$$

The multidimensional case with a binary mask gives

$$\arg \min_{\mathbf{z} \in \mathbb{C}^n} \frac{1}{2} \|\mathbf{z} - \mathbf{x}\|_2^2 + \frac{\lambda}{2} \|\mathbf{S}\mathbf{z} - \mathbf{y}\|_2^2 \quad (7)$$

$$= \mathbf{S} \left( \frac{1}{1+\lambda} \mathbf{x} + \frac{\lambda}{1+\lambda} \mathbf{y} e^{j \arg \mathbf{x}} \right) + (\mathbf{I} - \mathbf{S}) \mathbf{x}. \quad (8)$$

---

**Algorithm 1** Accelerated proximal gradient descent with restart

---

**Input:** Initialization  $\mathbf{x}_0 \in \mathbb{C}^n$ , stepsize  $\gamma$ , measurement noise level  $\sigma_{\mathbf{n}}$ , noise level  $\sigma$ , and tolerance  $\varepsilon > 0$

- 1: Set  $t_0 = 1, k = 0, r_0 = \infty, s_0 = \infty, \mathbf{z}_0 = \mathbf{x}_0$
- 2: **while**  $r_k > \varepsilon$  **do**
- 3:    $\mathbf{x}_{k+1} = \text{prox}_{\gamma f / \sigma_{\mathbf{n}}}(\mathbf{z}_k - \gamma \nabla R_{\sigma}(\mathbf{z}_k))$
- 4:    $s_{k+1} = R_{\sigma}(\mathbf{z}_k)$
- 5:    $t_{k+1} = \frac{1 + \sqrt{1 + 4t_k^2}}{2}$
- 6:    $\mathbf{z}_{k+1} = \mathbf{x}_{k+1} + \frac{t_k - 1}{t_{k+1}} (\mathbf{x}_{k+1} - \mathbf{x}_k)$
- 7:   **if**  $s_{k+1} > s_k$  **then**
- 8:      $\mathbf{z}_{k+1} = \mathbf{x}_{k+1}$
- 9:      $t_{k+1} = 1$
- 10:   **end if**
- 11:    $r_{k+1} = \|\mathbf{x}_{k+1} - \mathbf{x}_k\| / \|\mathbf{x}_{k+1}\|$
- 12:    $k \leftarrow k + 1$
- 13: **end while**

**Output:** Approximate solution  $\mathbf{x}_{k+1}$

---



---

**Algorithm 2** Plug-and-play with DRUNet

---

**Input:** Initialization  $\mathbf{x}_0 \in \mathbb{C}^n$ , number of steps  $K$ , regularization parameter  $\lambda$ , measurement noise level  $\sigma_{\mathbf{n}}$ , noise schedule  $\sigma_k$

- 1: Set  $k = 0$
- 2: **while**  $k < K$  **do**
- 3:    $\beta = \lambda \sigma_{\mathbf{n}}^2 / \sigma_k^2$
- 4:    $\mathbf{x}_{k+1} = \text{prox}_{f/\beta}(D_{\sigma_k}(\mathbf{x}_k))$
- 5:    $k \leftarrow k + 1$
- 6: **end while**

**Output:** Approximate solution  $\mathbf{x}_{k+1}$

---

This follows from the separability of the objective; entries with  $S_{kk} = 1$  use the scalar proximal operator (4) while entries where  $S_{kk} = 0$  use the identity mapping. Finally, by [21],

$$\text{prox}_{g(\mathbf{U}\cdot)}(\mathbf{x}) = \mathbf{U}^H \text{prox}_g(\mathbf{U}\mathbf{x}), \quad (9)$$

which yields (3).  $\square$

#### 3.2. Variational Methods

We minimize the sum of the data-fidelity term and a TV or MFoE regularizer. TV is a well-established handcrafted regularization technique. It promotes the sparsity of the gradients of the original image. MFoE, by contrast, learns the noise-dependent regularizer  $R_{\sigma} : \mathbb{R}^n \rightarrow \mathbb{R}_+$  such that, for any image  $\mathbf{x} \in \mathbb{R}^n$  and  $\mathbf{y} \sim \mathcal{N}(\mathbf{x}, \sigma^2 \mathbf{I})$ ,  $\text{prox}_{R_{\sigma}}(\mathbf{y}) \approx \mathbf{x}$ . The parameter  $\sigma$  adapts the regularizer to the noise level.

To extend both TV and MFoE to complex data, we regularize magnitude and normalized phase separately, as in

$$\mathcal{R}_{\sigma}(\mathbf{x}) = R_{\sigma}(|\mathbf{x}|) + R_{\sigma}\left(\frac{\arg(\mathbf{x})}{2\pi}\right). \quad (10)$$

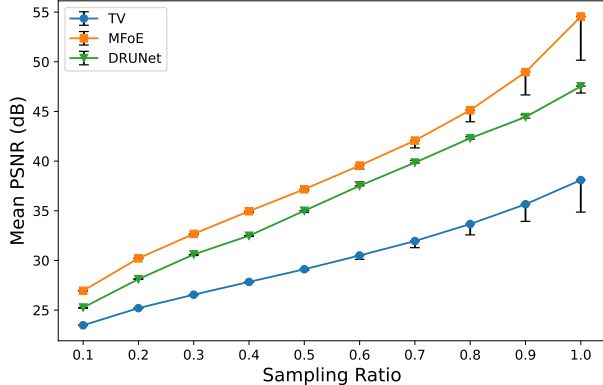


**Fig. 1.** PSNR (dB) for each model and sampling ratio without noise. Error bars show best, median, and worst performance over three random realizations on BSD68.

To get a reconstruction, we solve

$$\arg \min_{\mathbf{x} \in \mathbb{C}^n} \frac{1}{2\sigma_{\mathbf{n}}} \|\mathbf{SFD}\mathbf{x} - \mathbf{y}\|_2^2 + \lambda \mathcal{R}_{\sigma}(\mathbf{x}), \quad (11)$$

via accelerated proximal gradient descent with restart (Algorithm 1), using  $\gamma = 1/\text{Lip}(\nabla R_{\sigma})$ ,  $\varepsilon = 10^{-5}$ ,  $\lambda = 10^3$  for TV, and  $\lambda = 10^4$  for MFoE.

For TV, which does not depend on  $\sigma$ , we solve (11) once from complex Gaussian noise  $\mathbf{x}_0 \sim \mathcal{CN}(\mathbf{0}, \mathbf{I})$ . For MFoE, we exploit the noise parameter through a continuation scheme: we solve the problem three times, starting with  $\sigma = 1$ , then  $\sigma = 1/4$ , and finally  $\sigma = 1/16$ . The first run is initialized with  $\mathbf{x}_0 \sim \mathcal{CN}(\mathbf{0}, \mathbf{I})$ , subsequent runs with the previous solution. This progressively refines the reconstruction from coarse to fine. Additionally, in the first MFoE run, we down-weight the data-fitting term to avoid poor local minima—whenever  $\alpha > 0.25$ , we subsample  $\mathbf{S}$  to one quarter of its entries.

### 3.3. Plug-and-Play Methods

PnP approaches replace the explicit regularizer in an iterative reconstruction scheme with an off-the-shelf denoiser. We follow [11] and apply Algorithm 2 with DRUNet  $D_{\sigma}$ . To handle complex data, we split the signal into magnitude and phase, apply  $D_{\sigma}$  to both, and recombine.

The algorithm is initialized with  $\mathbf{x}_0 \sim \mathcal{CN}(\mathbf{0}, \mathbf{I})$  and uses  $\lambda = 0.23$  as in [11]. The noise schedule starts at  $\sigma_0 = 1$  and decreases geometrically to  $\sigma_K = 1/(1000\alpha)$ , where  $\alpha$  is the sampling ratio. Unlike the original work, which uses  $K = 8, 24$ , or  $40$ , we set  $K = 1000$ . The fact that this increase in the number of steps is necessary to achieve good reconstructions can be attributed to the nonlinear nature of our forward model, in contrast to the linear operators considered in [11]. We do not apply the data-fitting down-weighting strategy of MFoE for DRUNet as it does not result in performance improvements.

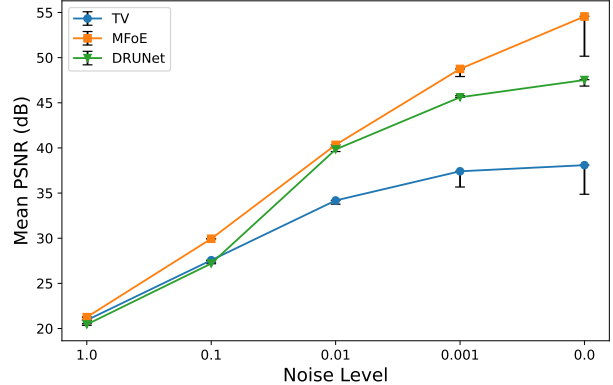


**Fig. 2.** PSNR (dB) for each model and noise level without subsampling. Error bars show best, median, and worst performance over three random realizations on BSD68.

## 4. EXPERIMENTS

To construct complex-valued signals, we start from real grayscale images, map pixel values in  $[0, 1]$  linearly to phases in  $[-\pi/2, \pi/2]$ , and assign unit magnitude. To assess robustness with respect to the forward model, we use three independently drawn diffusers and report the performance for all of them. The hyperparameters of Algorithms 1 and 2 were tuned on the Set12 dataset [22], while performance is reported on BSD68 [23].

Results for the noiseless subsampled case and the noisy case are shown in Figure 1 and Figure 2, respectively. Visual reconstructions are displayed in Figure 3. The metrics used to assess the performance of the reconstruction is the widely used peak signal-to-noise ratio (PSNR, higher is better). Interestingly, despite its state-of-the-art performance in denoising and multiple linear inverse problems, DRUNet is outperformed by MFoE in every setting. This suggests that the PnP framework may be suboptimal in the context of challenging nonlinear inverse problems.

For reference, plain gradient descent across all scenarios yields only about 4 dB of PSNR, which highlights the importance of image priors. Even a simple prior such as TV significantly boosts performance.

## 5. CONCLUSION

We investigated the benefit of image priors in the context of random phase retrieval with noise or extreme undersampling. We considered explicit regularizers (TV), learned explicit regularizers (MFoE), and implicit deep-learning-based priors (DRUNet). Our experimental results show that the incorporation of priors significantly improves reconstructions, even way below the weak recovery threshold. MFoE consistently outperforms TV and DRUNet, which highlights the effectiveness of learned explicit regularizers for challenging nonlinear inverse problems.



**Fig. 3.** Reconstruction results from TV, MFoE, and DRUNet. The reported metrics are (cosine similarity, PSNR).

## 6. REFERENCES

- [1] J. Dong, L. Valzania, A. Maillard, T.-a. Pham, S. Gigan, and M. Unser, "Phase retrieval: From computational imaging to machine learning: A tutorial," *IEEE Signal Processing Magazine*, vol. 40, no. 1, pp. 45–57, 2023.
- [2] C. Fienup and J. Dainty, "Phase retrieval and image reconstruction for astronomy," *Image Recovery: Theory and Application*, vol. 231, p. 275, 1987.
- [3] J. Miao, P. Charalambous, J. Kirz, and D. Sayre, "Extending the methodology of x-ray crystallography to allow imaging of micrometre-sized non-crystalline specimens," *Nature*, vol. 400, no. 6742, pp. 342–344, 1999.
- [4] L. Valzania, J. Dong, and S. Gigan, "Accelerating ptychographic reconstructions using spectral initializations," *Optics Letters*, vol. 46, no. 6, pp. 1357–1360, 2021.
- [5] G. Zheng, R. Horstmeyer, and C. Yang, "Wide-field, high-resolution Fourier ptychographic microscopy," *Nature Photonics*, vol. 7, no. 9, pp. 739–745, 2013.
- [6] L.-H. Yeh, J. Dong, J. Zhong, L. Tian, M. Chen, G. Tang, M. Soltanolkotabi, and L. Waller, "Experimental robustness of Fourier ptychography phase retrieval algorithms," *Optics Express*, vol. 23, no. 26, pp. 33 214–33 240, 2015.
- [7] M. Mondelli and A. Montanari, "Fundamental limits of weak recovery with applications to phase retrieval," in *Conference on Learning Theory*, 2018, pp. 1445–1450.
- [8] A. Maillard, B. Loureiro, F. Krzakala, and L. Zdeborová, "Phase retrieval in high dimensions: Statistical and computational phase transitions," *Advances in Neural Information Processing Systems*, vol. 33, pp. 11 071–11 082, 2020.
- [9] Z. Hu, J. Tachella, M. Unser, and J. Dong, "Structured random model for fast and robust phase retrieval," in *IEEE International Conference on Acoustics, Speech and Signal Processing*, 2025, pp. 1–5.
- [10] L. I. Rudin, S. Osher, and E. Fatemi, "Nonlinear total variation based noise removal algorithms," *Physica D: Nonlinear Phenomena*, vol. 60, no. 1, pp. 259–268, 1992.
- [11] K. Zhang, Y. Li, W. Zuo, L. Zhang, L. Van Gool, and R. Timofte, "Plug-and-play image restoration with deep denoiser prior," *IEEE Transactions on Pattern Analysis and Machine Intelligence*, vol. 44, no. 10, pp. 6360–6376, Oct. 2022.
- [12] S. Hurault, A. Leclaire, and N. Papadakis, "Gradient step denoiser for convergent plug-and-play," in *International Conference on Learning Representations*, 2022.
- [13] A. Goujon, S. Neumayer, P. Bohra, S. Ducotterd, and M. Unser, "A neural-network-based convex regularizer for inverse problems," *IEEE Transactions on Computational Imaging*, vol. 9, pp. 781–795, 2023.
- [14] S. Ducotterd and M. Unser, "Multivariate fields of experts," *arXiv:2508.06490*, 2025.
- [15] P. Hand, O. Leong, and V. Voroninski, "Phase retrieval under a generative prior," *Advances in Neural Information Processing Systems*, vol. 31, 2018.
- [16] P. Bohra, T.-a. Pham, J. Dong, and M. Unser, "Bayesian inversion for nonlinear imaging models using deep generative priors," *IEEE Transactions on Computational Imaging*, vol. 8, pp. 1237–1249, 2023.
- [17] E. Bostan, R. Heckel, M. Chen, M. Kellman, and L. Waller, "Deep phase decoder: Self-calibrating phase microscopy with an untrained deep neural network," *Optica*, vol. 7, no. 6, pp. 559–562, 2020.
- [18] B. Zhang, W. Chu, J. Berner, C. Meng, A. Anandkumar, and Y. Song, "Improving diffusion inverse problem solving with decoupled noise annealing," in *Proceedings of the Computer Vision and Pattern Recognition Conference*, 2025, pp. 20 895–20 905.
- [19] Çağatay Işil and F. S. Oktem, "Deep plug-and-play HIO approach for phase retrieval," *Applied Optics*, vol. 64, no. 5, pp. 84–94, Feb 2025.
- [20] A. Denker, J. Hertrich, Z. Kereta, S. Cipiccia, E. Erin, and S. Arridge, "Plug-and-play half-quadratic splitting for ptychography," in *Scale Space and Variational Methods in Computer Vision*, 2025, pp. 269–281.
- [21] P. L. Combettes and J.-C. Pesquet, "Proximal splitting methods in signal processing," in *Fixed-Point Algorithms for Inverse Problems in Science and Engineering*, 2011, pp. 185–212.
- [22] K. Zhang, W. Zuo, Y. Chen, D. Meng, and L. Zhang, "Beyond a Gaussian denoiser: Residual learning of deep CNN for image denoising," *IEEE Transactions on Image Processing*, vol. 26, no. 7, pp. 3142–3155, 2017.
- [23] D. Martin, C. Fowlkes, D. Tal, and J. Malik, "A database of human segmented natural images and its application to evaluating segmentation algorithms and measuring ecological statistics," in *IEEE International Conference on Computer Vision*, vol. 2, 2001, pp. 416–423.